Note on the Calculation of the Spherically Aberrated Field of an Acoustic Lens

by Terence A. Cornelius and Kevin L. Williams

Technical Memorandum
APL-UW TM7-92
September 1992

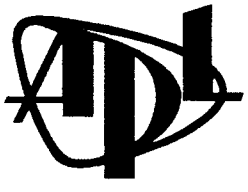

Applied Physics Laboratory University of Washington
1013 NE 40th Street Seattle, Washington 98105-6698

Contract N00039-91-C-0072

REPORT DOCUMENTATION PAGE

Form Approved
OMB No. 0704-0188

1a. REPORT SECURITY CLASSIFICATION
Unclassified

1b. RESTRICTIVE MARKINGS

2a. SECURITY CLASSIFICATION AUTHORITY

3. DISTRIBUTION / AVAILABILITY OF REPORT
Approved for public release;
distribution unlimited.

2b. DECLASSIFICATION / DOWNGRADING SCHEDULE

4. PERFORMING ORGANIZATION REPORT NUMBER(S)
APL-UW TM 7-92

5. MONITORING ORGANIZATION REPORT NUMBER(S)

6a. NAME OF PERFORMING ORGANIZATION
Applied Physics Laboratory
University of Washington

6b. OFFICE SYMBOL (*If applicable*)

7a. NAME OF MONITORING ORGANIZATION

6c. ADDRESS (*City, State, and ZIP Code*)
1013 N.E. 40th Street
Seattle, WA 98105-6698

7b. ADDRESS (*City, State, and ZIP Code*)

8a. NAME OF FUNDING / SPONSORING ORGANIZATION
Defense Nuclear Agency

8b. OFFICE SYMBOL (*If applicable*)

9. PROCUREMENT INSTRUMENT IDENTIFICATION NUMBER
SPAWAR N00039-91-C-0072

8c. ADDRESS (*City, State, and ZIP Code*)
6801 Telegraph Road
Alexandria, VA 22310-3398

10. SOURCE OF FUNDING NUMBERS

PROGRAM ELEMENT NO.	PROJECT NO.	TASK NO.	WORK UNIT ACCESSION NO.

11. TITLE (*Include Security Classification*)
Note on the Calculation of the Spherically Aberrated Field of an Acoustic Lens

12. PERSONAL AUTHOR(S)
T.A. Cornelius and K.L. Williams

13a. TYPE OF REPORT	13b. TIME COVERED	14. DATE OF REPORT (*Year, Month, Day*)	15. PAGE COUNT
Technical	FROM _____ TO _____	September 1992	40

16. SUPPLEMENTARY NOTATION

17 COSATI CODES			18. SUBJECT TERMS (*Continue on reverse if necessary and identify by block number*)
FIELD	GROUP	SUB-GROUP	Spherical aberration Caustic Acoustic lens

19. ABSTRACT (*Continue on reverse if necessary and identify by block number*)

A treatment of the propagation of plane sound waves into a hemispherical acoustic lens is presented—first, in terms of geometrical acoustics, showing the utility and the limitations of that approach, and then in terms of a hybrid approach that incorporates geometrical acoustics and wave acoustics. The nature of the spherical aberration that characterizes such systems is investigated, and special attention is paid to the caustics formed. The main result is the determination of the pressure field in the vicinity of the focusing region of the lens. The spherically aberrated field has an ellipsoidal shaped focusing region; its shape is determined by the relative sound speeds of the water external to the lens and the lens fluid.

20. DISTRIBUTION / AVAILABILITY OF ABSTRACT
☒ UNCLASSIFIED/UNLIMITED ☒ SAME AS RPT. ☐ DTIC USERS

21. ABSTRACT SECURITY CLASSIFICATION
Unclassified

22a. NAME OF RESPONSIBLE INDIVIDUAL
LT Michael Guarracino

22b. TELEPHONE (*Include Area Code*)
(703) 325-1002

22c. OFFICE SYMBOL
Code NSNS

Table of Contents

I. Introduction

A treatment of the propagation of plane sound waves into a hemispherical acoustic lens is presented—first, in terms of geometrical acoustics, showing the utility and the limitations of that approach, and then in terms of a hybrid approach that incorporates geometrical acoustics and wave acoustics. The nature of the spherical aberration that characterizes such systems is investigated, and special attention is paid to the caustics formed.

Acoustics includes the study of sound and sound-like phenomena—especially mechanical radiation in fluids. Thus, it can be seen as part of the mechanics of continuous media, which tends to concentrate less upon the bulk motions of the medium than upon the temporal behavior of pressure fields in the medium. It is inherently a difficult subject, rarely giving results that are simultaneously intuitively clear, computationally simple, and analytically exact. Two of the general approaches to acoustics are geometrical acoustics and wave acoustics. The former emphasizes intuitive clarity and computational simplicity, but is acceptably accurate only in a fairly restricted domain. The latter approach is considerably more rigorous and has a much broader domain, but is intuitively and computationally difficult.

An acoustic lens refracts sound. When mechanical waves encounter a boundary between two distinct media they may partially or totally reflect from the boundary, and the transmitted waves may change their direction of propagation. The extent to which these effects take place depends upon the media involved and the direction of the sound's propagation with respect to the boundary surface, among other things.

The particular acoustic lens treated in greatest detail here is the University of Washington Applied Physics Laboratory's Acoustic Lens Sonar. Designed to be immersed in water, it consists of an acoustically transparent shell, a fluid-filled cavity, and a retina on which is installed an array of transducers (Fig. 1).

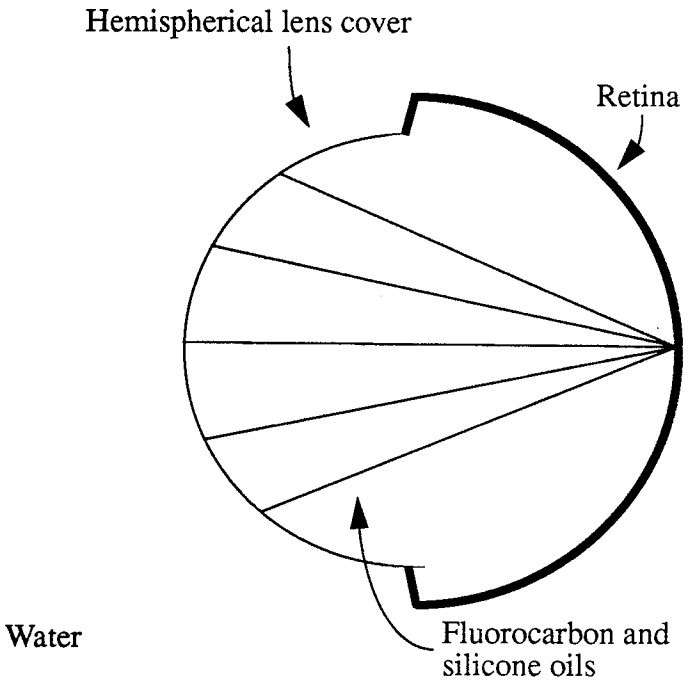

FIG.1. An APL-UW acoustic lens sonar

This system has many practical advantages over alternative sonars of similar abilities, but it has disadvantages due ultimately to the properties of focusing acoustical systems—i.e., aberrations in focusing. It turns out that the structure of the refracted wavefield in the focusing region is very complex, and that this structure changes in unsuspected ways with variations in the system's temperature, or with the nature of the oils filling the lens. That is, the focusing changes with variations in the system's refractive indices. These variations can make interpretations of signals from the retina difficult. What is required is a better understanding of the wavefield in the focusing region of such systems. That is what is provided in this report; further, the results and material covered are applicable in many cases beyond the Applied Physics Laboratory's acoustic lens.

A sketch of the geometrical approach to acoustics, in the form used here, includes the following elements. Its domain is restricted to cases when media are isotropic, pressure amplitudes are small and slowly varying in space and time, and such wave phenomena as interference and diffraction are not of interest. Two complementary pictures are distinguished: the ray picture, in which there is a clear analogy to beam optics; and the wavefront picture, where one can make an analogy to the behavior of surface waves—say, water waves. Basic tools of geometrical acoustics include Fermat's principle, Snell's law, the Huygens construction, and the Law of Reflection.

Wave acoustics, in the form used here, has a much less restricted domain. Applicable cases are those where the properties of the medium are independent of space and time; where linear approximations to the basic equations of fluid mechanics can be used; where disturbances in the medium have small amplitudes; and where the absorption of sound is not of interest. With these restrictions, the wave equation familiar from other areas of physics can be applied to acoustics, together with well-understood techniques for its solution in important cases.

II. Geometrical Acoustics of Reflectors and Lenses

Section II is introduced by a brief discussion of elementary concepts of geometrical acoustics. In II. A we examine an acoustic reflector, or mirror; in II. B an acoustic lens; and in II. C the caustic region, where focusing occurs and geometrical acoustics fails.

The ray picture of geometrical acoustics approximates waves by rays. Rays are lines drawn in space corresponding to the direction of the flow of acoustical energy. In an isotropic medium, rays are orthogonal trajectories of the waveforms—i.e., lines everywhere normal to the wavefronts. Within homogeneous isotropic materials, rays will be straight lines. This follows by symmetry, there being no preferred direction in such media. In the geometrical approximation, the behavior of rays is governed by the Law of Reflection and Snell's law. Computations involving these laws are not difficult. With both, the analogy to light rays is obvious, and encourages intuitive understanding of some of the processes involved. The limitations of the approach are discussed after its utility is suggested.[1]

1. See Section II.C.

A. Acoustic mirror

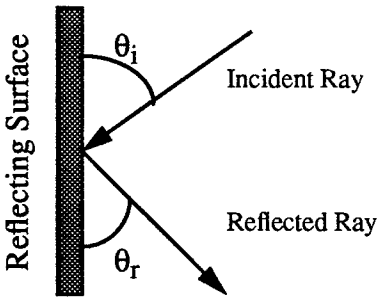

FIG. 2. Terms for the Law of Reflection

The Law of Reflection holds that any reflection is such that the angle of an incident ray with respect to a reflecting surface, θ_i, is equal to the angle of a reflected ray with respect to the reflecting surface, θ_r, and the incident and reflected rays are in the same plane (Fig. 2).

An acoustic mirror, or reflector, can be treated as an elementary application of the Law of Reflection. The mirror is a surface from which it is assumed that essentially all incident rays reflect. In what follows, the mirror's shape is taken to be that of a surface of revolution symmetrical about the z-axis. The mirror's section in the x-z plane is given by

$$x = Az^2 + Bz^4 \qquad (1)$$

where A and B are adjustable real-number parameters. Using this method of specifying the mirror's profile, we can, to second order, approximate many profiles symmetrical across the x-axis. The family of such cases includes two cases of particular importance: the parabola, which is given exactly by letting A be nonzero while B is zero; and the semicircle, which for a given radius can be approximated for appropriate choices of A and B.[2] Here and throughout, we will assume that the incident rays are all parallel to each other and to the z-axis, and that their direction is such that reflected or refracted rays propagate generally from the negative z-direction toward the positive z-direction—i.e., from left to right.

Suppose the reflecting surface has a parabolic section given by $x = z^2$, i.e., $A = 1$ and $B = 0$. For the portion of the mirror near the z-axis we obtain the following pattern of reflected rays.

2. See text immediately preceding Section II.B.

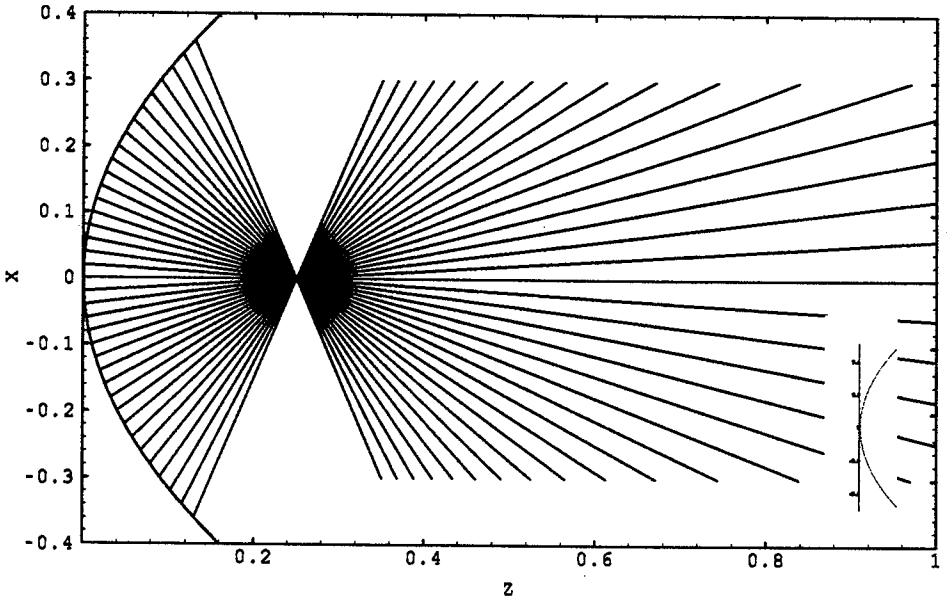

FIG. 3. Reflections from a paraboloidal surface[3]

It is notable that all the reflected rays pass through the same point, the focal point. It is logical that any change of the reflector's profile will produce defocusing. The object here is to understand that defocusing qualitatively and, later, quantitatively. (The small inset diagrams in Figures 3 through 8 exhibit the profiles of the reflecting surfaces, usually in comparison to some simple, reference surface. In Figure 2, the reflector is itself a simple surface. In Figures 4 through 7, the inset figure is a comparison of the reflector's profile with the profile of the reflector in Figure 3, i.e., with a parabola.)

Introducing an admixture of z^4 with a small, negative coefficient into the equation describing the reflector's profile can be seen qualitatively to lead to one sort of defocusing. Consider Figures 4 and 5. Heuristically, we can explain the patterns in this way: the more $-x^4$ that is introduced, the farther the edges of the reflector bend back; as the edges of the reflector bend farther back, the rays incident there reflect in a direction more nearly parallel to the x-axis.

It might be expected that, were the edges of the reflector to bend farther in, the rays incident there would reflect in a direction more nearly parallel to the z-axis, or even antiparallel to the positive x-axis; that is the case, as shown below. Figure 6 shows a relatively extreme case.

3. See Appendix A for a discussion of how Figures 3 through 8 were generated.

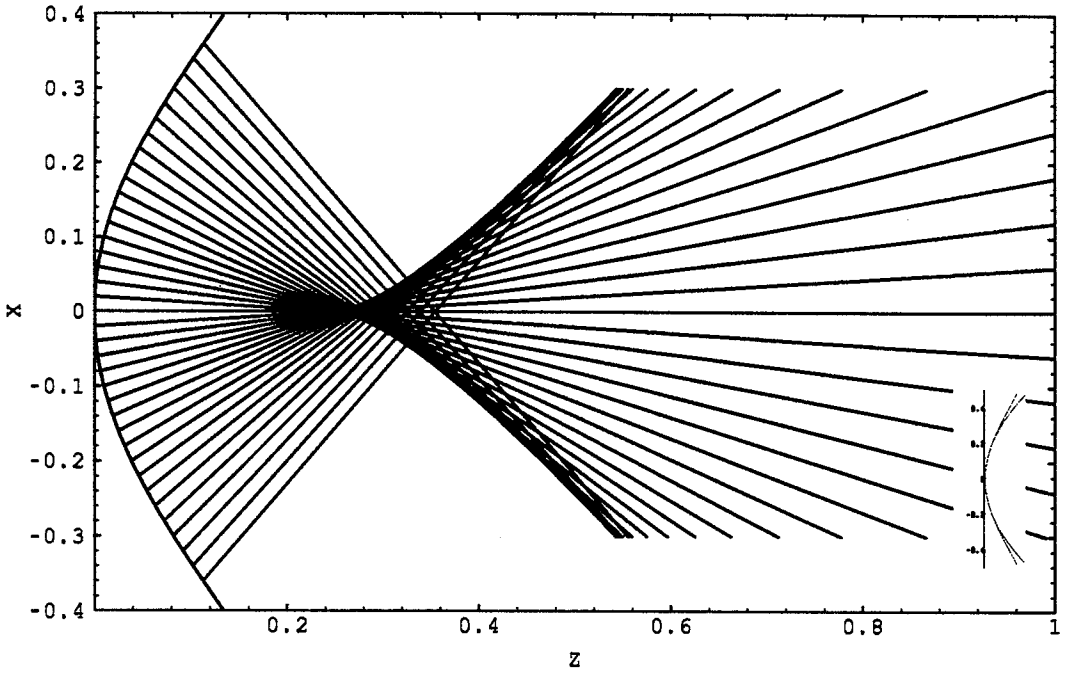

FIG. 4. Reflections from the surface with profile $x = z^2 - z^4$

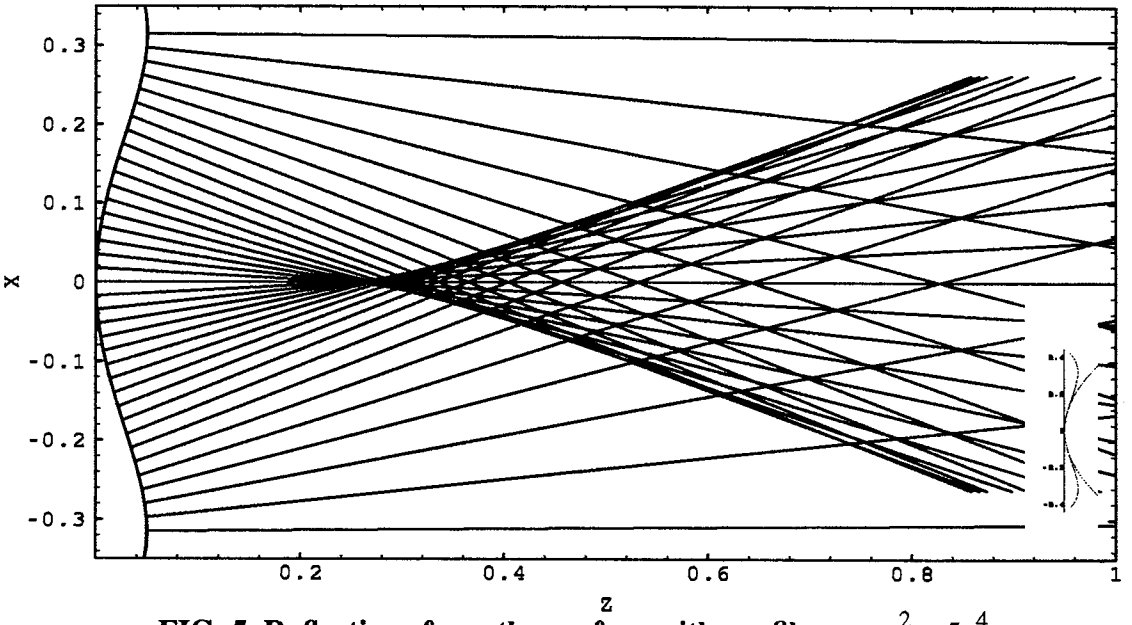

FIG. 5. Reflections from the surface with profile $x = z^2 - 5z^4$

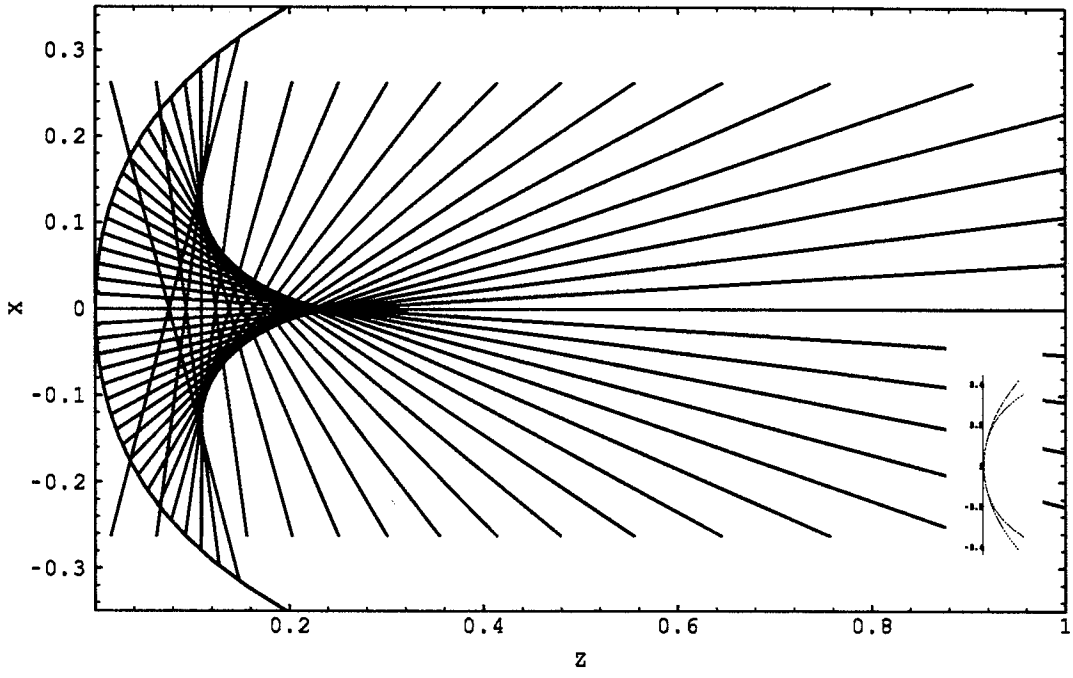

FIG. 6. Reflections from the surface with profile $x = z^2 + 5z^4$

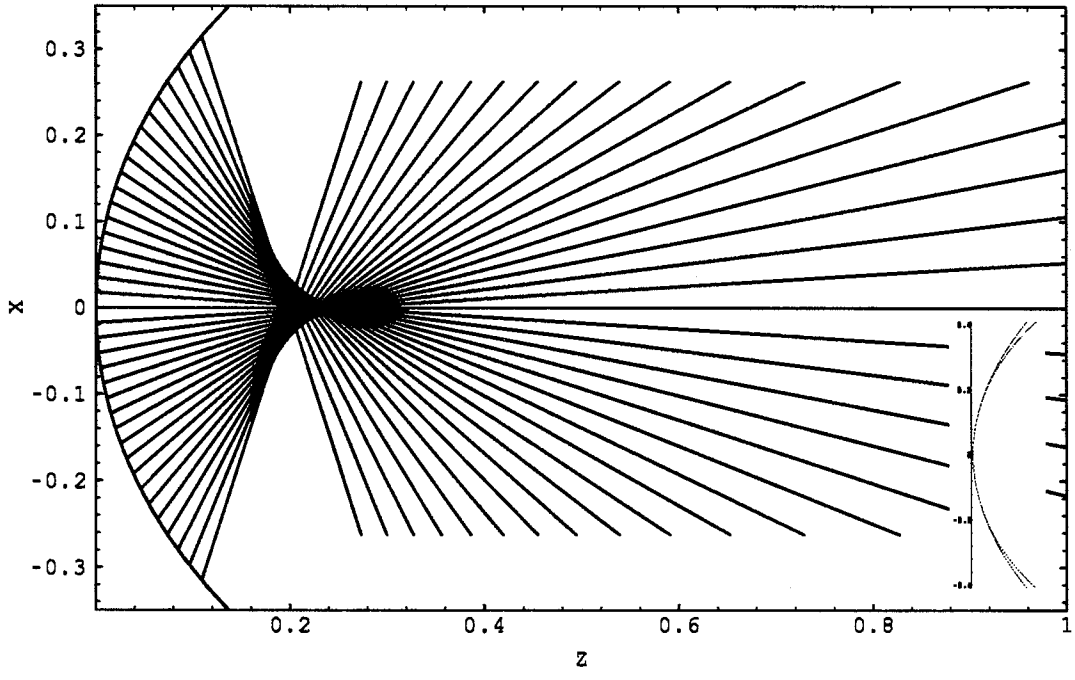

FIG. 7. Reflections from the surface with profile $x = z^2 + z^4$

Figure 7 is a case of special interest for our present purposes. Notice that the profile of this reflector resembles the arc of a circle. Analytically, we might expect this to be the case. An equation for

a circle of radius r in the x-z plane, with its center at the origin, is $r^2 = x^2 + z^2$, or $\pm x = \sqrt{r^2 - z^2}$. For $z \ll r$, we can approximate

$$x \approx \pm\left(r - \frac{1}{2r}z^2 - \frac{1}{8r^3}z^4\right). \tag{2}$$

If we ignore offsets in the x- and z-directions, we can make this correspondence:

$$Az^2 + Bz^4 \leftrightarrow \frac{1}{2r}z^2 + \frac{1}{8r^3}z^4. \tag{3}$$

This suggests that $A \leftrightarrow \frac{1}{2r}$ and $B \leftrightarrow \frac{1}{8r^3}$. Choosing $r = \frac{1}{2}$ gives $A = B = 1$. Thus, reflections from the surface with profile $x = z^2 + z^4$ should resemble those from a concave spherical sector of radius 1/2. Figure 8 shows such reflections.

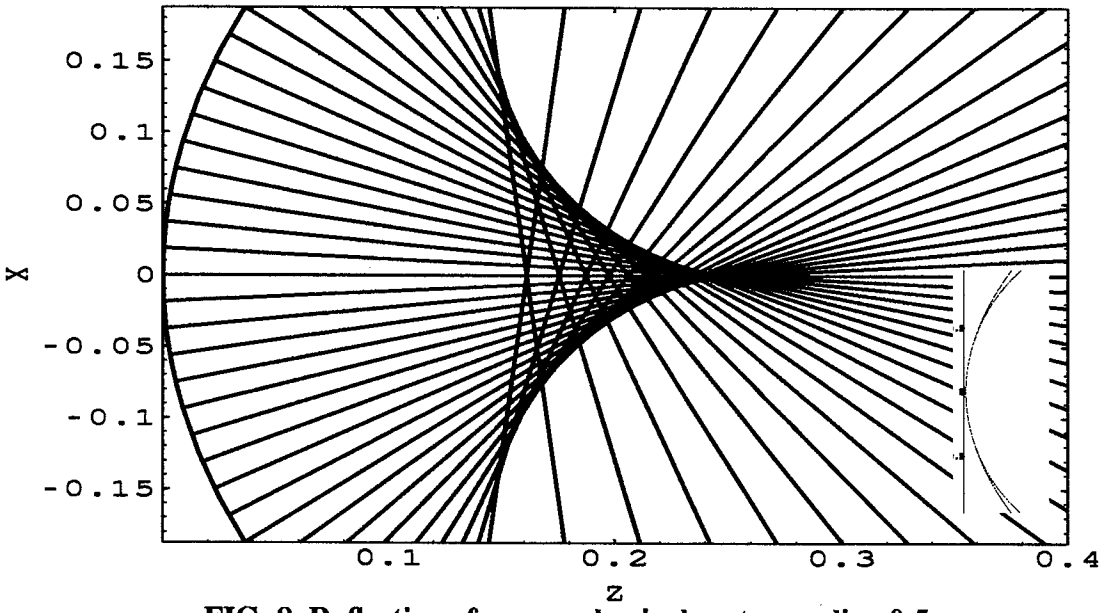

FIG. 8. Reflections from a spherical sector, radius 0.5

As the argument above suggests, the divergence between the reflections shown in Figures 7 and 8 is largest near the edges of the reflector. But in the axial region, the correspondence is remarkably close. Here the inset shows a comparison of the semicircle with the surface $x = z^2 + z^4$.

B. Acoustic lens

We now turn to the examination of an acoustic lens. Snell's law holds that

$$\sin\theta = M \sin\nu, \tag{4}$$

where

θ is the angle of incidence
ν is the angle of refraction

$M = c/c_i$, the acoustic index of refraction

c_i is the sound velocity in the refracted or inner medium

c is the sound velocity in the incident or outer medium.

Again, the incident and refracted rays are taken to be in the same plane.

.

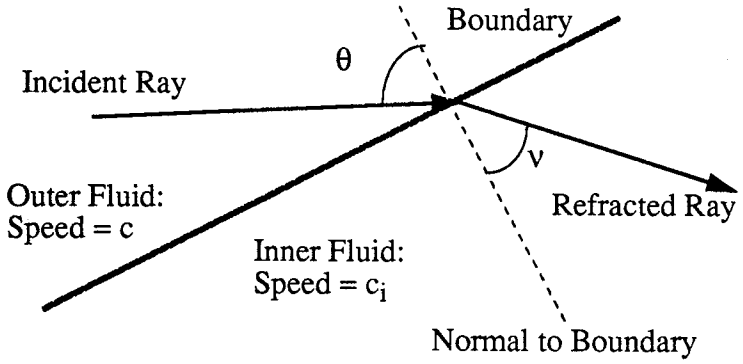

FIG. 9. Terms for the Law of Refraction

The case of the acoustic lens can be treated as an application of Snell's law. Inspection of this law makes it obvious that, with $c > c_i$, θ must be greater than ν: that is, the ray refracts toward the normal to the boundary. If the boundary is convex with respect to the outer fluid, then the boundary can act as a thick lens, causing rays incident on the outside to converge on the inside. Again, consider rays parallel to the principal axis of the system, now incident from the left, or negative z-direction. Figure 10 shows the pattern of refractions in a hemispherical lens, where the sound speed ratio c_i/c is about 0.6.

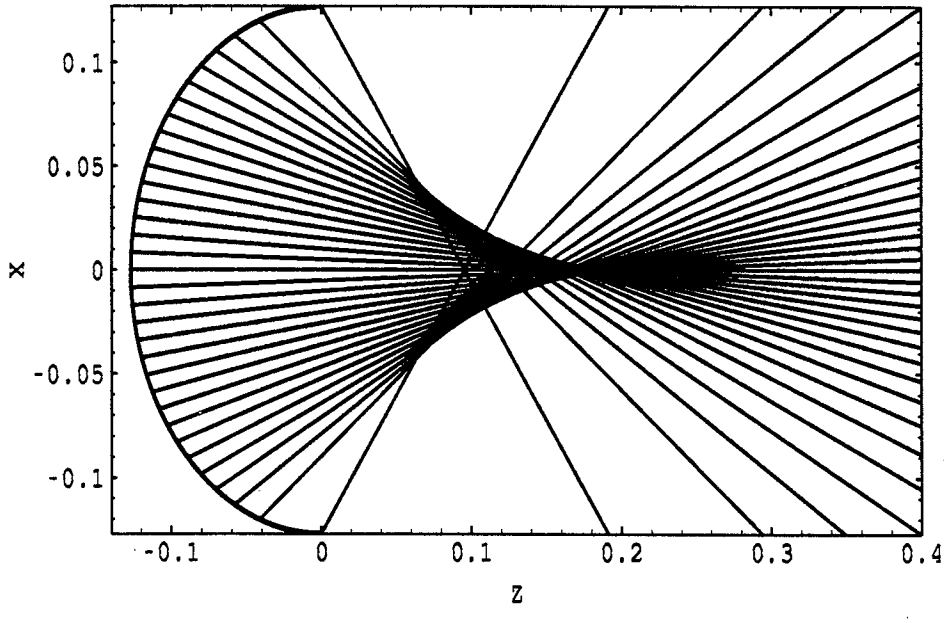

FIG. 10. Refractions in a hemispherical lens, c_i/c = 844.1/1404

Again, we notice a considerable degree of aberration; the rays incident at the edges of the lens

are refracted "too far" in comparison to those nearer the lens's vertex. As in the case of a reflector whose profile was the arc of a circle, there is a caustic curve that opens toward the element's surface. Changing the ratio c_i/c changes the pattern. For example, a ratio about half as great reduces the aberration, as seen in Figure 11.

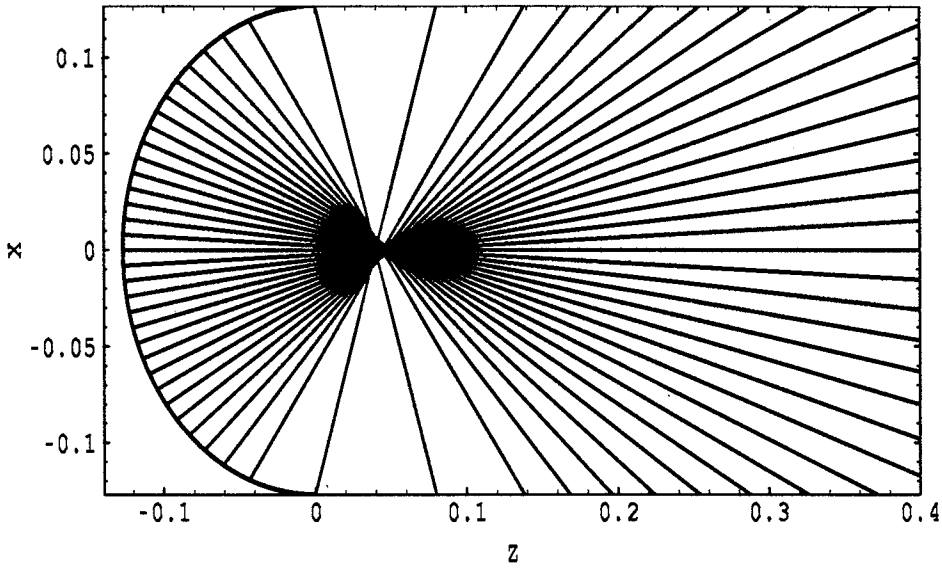

FIG. 11. Refractions in a hemispherical lens, $c_i/c = 0.30$

As the ratio c_i/c approaches zero, the refracted rays lie more nearly upon the normals to the surface: for a hemisphere, the normals are radii, so the refracted rays come more nearly to a focus at the sphere's center. As the ratio approaches 1, the refracted rays are more nearly parallel to the incident rays, and the degree of aberration increases.

C. The caustic region

The pattern of reflected or refracted rays that is produced can be characterized by the *caustic* formed. A caustic is the envelope of reflected (or refracted) rays produced by rays emanating from a given object point. Caustics are produced by most reflecting or refracting systems, but we will restrict ourselves to those produced by spherical lenses and reflectors. See Figure 12.

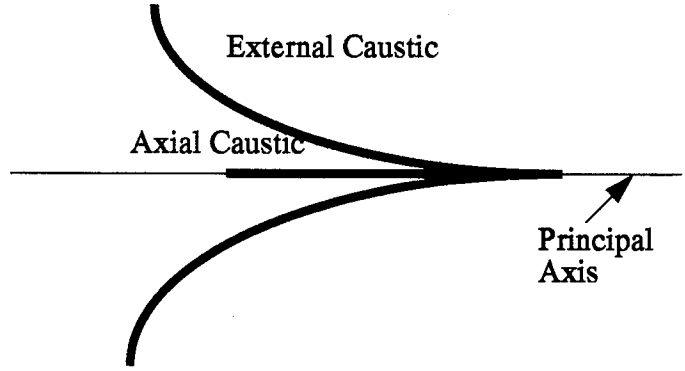

FIG. 12. Caustic curves for rays reflected from a concave spherical surface[4]

We see a cusped curve embracing an axial "spike." The external caustic is easily seen to be the curve to which the reflected (or refracted, for a lens) rays are tangent, as for example in Figure 7. Of course, caustics are three-dimensional. The external caustic, when revolved around the principal axis, assumes a flared or trumpet-like shape. The central caustic remains a spike. Not obvious from a two-dimensional illustration is the source of the "spike," or central caustic. Consider that each annular ring centered on the principal axis of the reflector's (or lens's) surface must reflect (or refract) all its rays through the same point on the principal axis: the central caustic is the locus of points from all such annular rings. Reviewing the reflected and refracted ray diagrams above, one immediately notices that the details of these caustics are sensitively dependent upon the characteristics of the system that gives rise to them: their extent, their curvature, and even the direction in which they open, are all variable. (The pattern for the parabolic reflector shows no caustic, but, for a variety of reasons, it is most useful to view this not as the absence of a caustic but as a special case of a caustic—a point caustic.[5]) In the other cases, caustics inhabit the focal regions of the systems. Characterizing the caustic is a way of characterizing one important sort of aberration in the system.

Caustics can be exhibited, as we have done, using the most elementary geometrical methods. Mathematical extensions of the geometrical methods used above can give a precise spatial characterization of the caustics produced in a system, especially in the simple cases we have treated. Caustic regions can be located, their dimensions and curvatures can be specified, and so forth.[6] However, geometrical acoustics cannot give a richer, more physical description of the caustics—these methods do not permit one sensibly to describe what happens in these regions.

As a simple, but important, example, consider the energy density on the central caustic. Each infinitesimal length on the central spike concentrates the rays from an annular ring of the system's surface. Since each point on the ring can give rise to a ray, and there is an infinity of points on the ring, each point on the spike must be the intersection of an infinity of rays. If these rays relate somehow to the flow of energy, then the energy densities in the neighborhood of the central spike

4. See Appendix C for a discussion of the method used to generate the curve in Figure 12.

5. For example "tweaking" the profile of the parabolic reflector slightly — as in Figure 3 and 5— produces the characteristic caustic. An ellipsoidal lens is also capable of forming an analogous point caustic, for an object point on axis and for the proper choice of parameters.

6. See Appendix C for one example.

diverge in a very unphysical way. Even taking the central spike to have some small but finite surface area—which, in terms of the model, it does not—does not save us. For the energy densities on the spike can quickly exceed the energy densities near the object point, in violation of the principles of thermodynamics. And this is not to speak of the physical behavior of the fluid in which the sound is propagated. How does the material medium stand up to these indefinite energy densities? What happens to the amplitude of the disturbances we know to be propagating through the caustic region? There are a great many such questions.

Sound is a wave: the geometrical acoustics method abstracts that fact away. We must turn to a richer and more physical description of the acoustic lens if we want a coherent picture of what happens in the caustic region—that is, near the system's focus. Our approach is to combine the geometrical acoustics picture used above with a simple wave acoustics picture to locate the caustic. We turn to the full complexities of wave acoustics only to describe the behavior of the system in the caustic region.

III. Hybrid Geometrical Acoustics/Wave Acoustics Approach

In Section III. A, we will present relations useful in finding the structure of the caustic for a spherical acoustic lens—the "skeleton" of the wavefield, as it were—and the wavefield structure that "covers" the skeleton. Then we will describe the use of these relations and show some representative results. For the region relatively far from the caustic and its complications, the geometrical approach will be used to determine the propagation of sound toward the caustic region: the computations are simple and easy to interpret, as suggested in Section II. For the region near the caustic, we shift to the full Kirchhoff calculation of the wavefield: this is more complex and difficult to visualize, but it is required where the wave nature of sound can not be ignored. While no component of this hybrid approach is novel, this combining of approaches has the advantage of giving a physical insight into the breakdown of the geometrical acoustics approximation. In Section III.B, we discuss preliminaries to the wave calculations we have employed; in III.C, we sketch the calculations themselves and present some representative results.

A. Caustic structure

We now shift the focus from rays to wavefronts. A wavefront is any moving surface along which a waveform feature is being simultaneously received.[7] For a periodic wave, this amounts to saying that a wavefront is a surface of constant phase. A plane wave incident upon a spherical converging lens gives rise to a convex curved—but aspherical—refracted wavefront in the lens's interior. Near any given point on the wavefront its surface can be approximated by the surface of

7. See, e.g., A. D. Pierce, *Acoustics: An Introduction to Its Principles and Applications* (McGraw-Hill, New York, 1981), p. 371, for a slightly more formal definition of "wavefront."

an appropriately chosen tangent sphere. The curvature of the wavefront at that point can be expressed in terms of the radius of the tangent sphere. A more-sharply curved section of the wavefront is more closely approximated by a sphere of smaller radius.[8] Rays travel in the direction of the radii of such spheres that are tangent to the wavefront. See Figure 13.

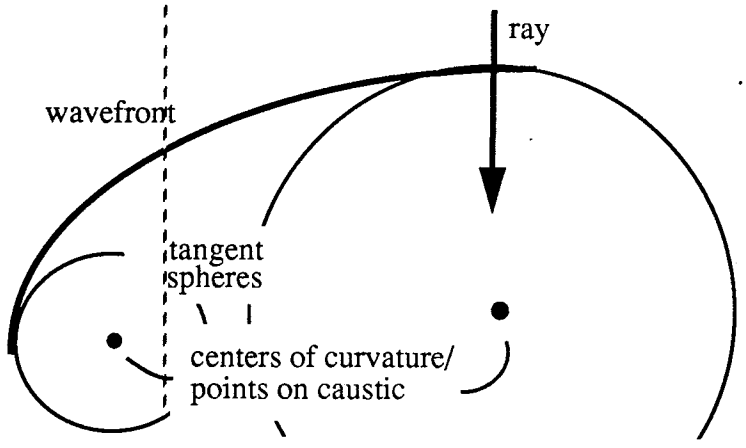

FIG. 13. Wavefronts, rays, and points on caustic curve

In terms of the geometry of wavefronts, the caustic is the locus of the centers of all such spheres. This is equivalent to saying that the caustic is the locus of the intersections of the refracted rays. The wavefront picture is less easily visualized than the ray picture, but the apparatus used in the mathematical formulation of the wavefront picture is more suitable to the present hybrid approach. We now sketch a development of expressions for the centers of curvature of the refracted wavefront—i.e., for points on the caustic surface. Figure 14 defines our terms.

8. To be more precise, the curvature of the wavefront in a given plane normal to the wavefront can be approximated by the curvature of such a tangent sphere. Notice that the curvature in one normal plane need not be the same as in another normal plane. Consider a saddle-shaped wavefront propagating to the right. Its curvature might be convex in the vertical normal plane, but concave in the horizontal normal plane. Differential geometry explores such matters. See any general work on the subject.

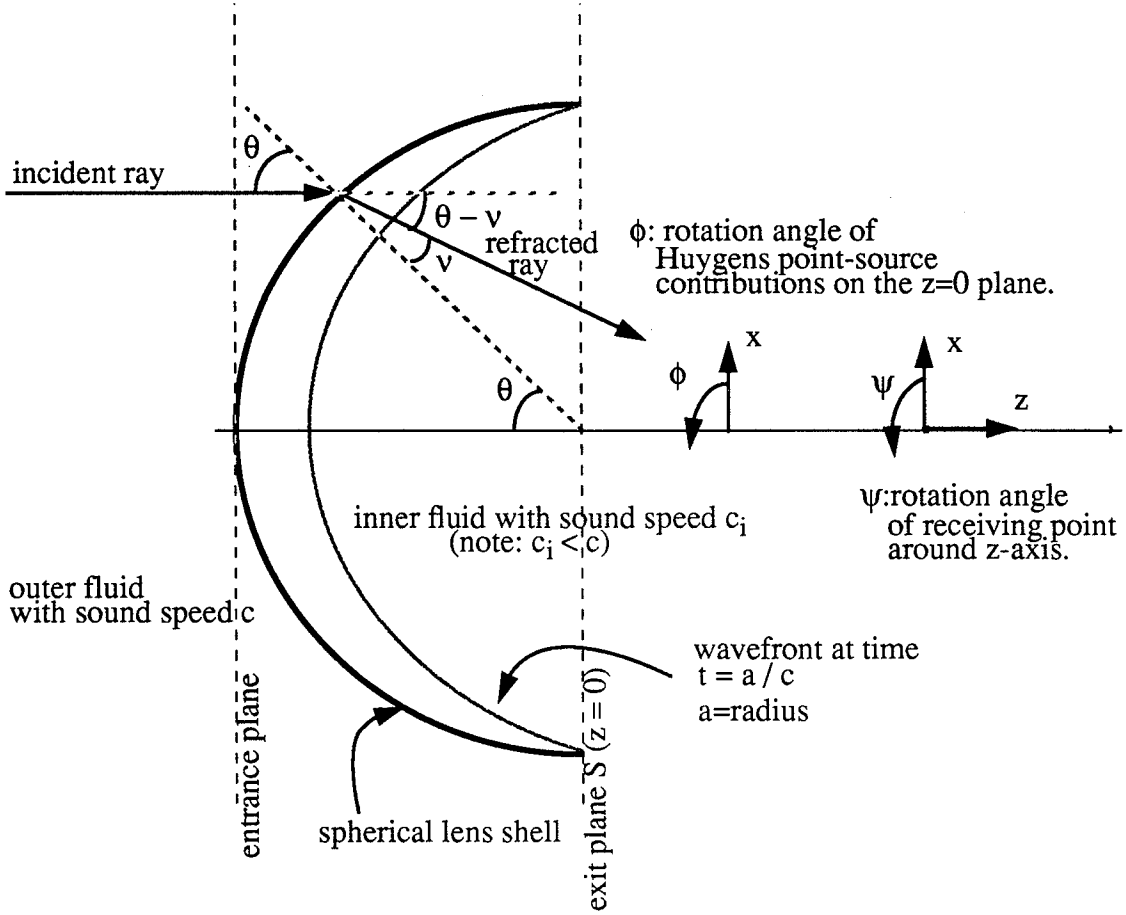

FIG. 14. Some terms of reference for Section III

First, we want to determine the propagation of the wavefront in the lens. Here $W(\theta, t_i)$ is the distance in the z-direction behind the exit plane of a given infinitesimal section of the refracted wavefront at a given time t_i, and $h(\theta, t_i)$ is the corresponding distance in the x-direction above the z-axis, with θ the angle that characterized the point at which the section of wavefront was transmitted through the lens surface.[9] For convenience we set the time equal to zero when the incident plane wave is at the entrance plane. We will calculate $W(\theta)$ and $h(\theta)$ at time $t = a/c$, which is the time the section of the wavefront incident at the edge of the lens ($\theta = \pm\pi/2$) reaches the exit plane. (We can equally well say θ is the ray's angle of incidence and t is the time required for the marginal ray to reach the exit plane.) See Figure 15.

9. The symmetry of the problem allows us to use just one angle parameter to define the spatial section of the wavefront. In the actual calculation of the caustic, we have used Snell's law to express W in terms of ν rather than θ. This is a matter of computational convenience rather than mathematical necessity. See Appendix D.

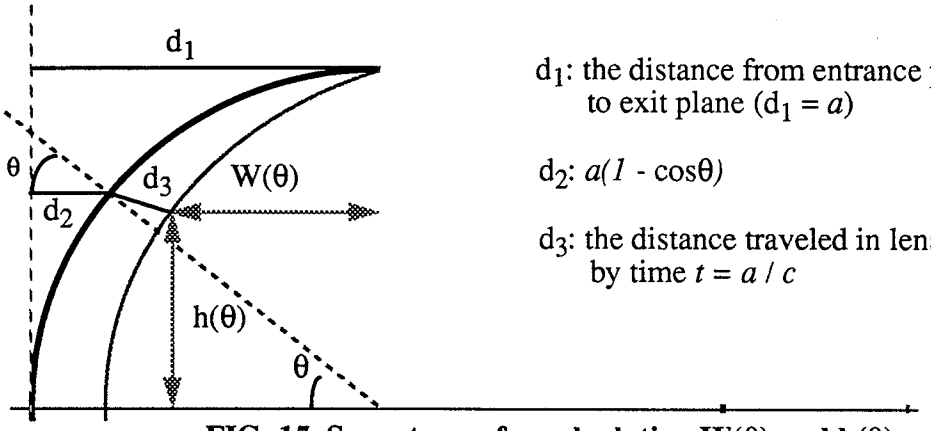

d_1: the distance from entrance plane to exit plane ($d_1 = a$)

d_2: $a(1 - \cos\theta)$

d_3: the distance traveled in lens by time $t = a / c$

FIG. 15. Some terms for calculating W(θ) and h(θ)

From the foregoing we have

$$t = a/c \tag{5}$$

and (because $t = d_2/c + d_3/c_i$)

$$t = \frac{a(1-\cos\theta)}{c} + \frac{d_3}{c_i}. \tag{6}$$

Equating, we have

$$\frac{a}{c} = \frac{a(1-\cos\theta)}{c} + \frac{d_3}{c_i}, \tag{7}$$

which implies

$$d_3 = \frac{c_i}{c} a\cos\theta. \tag{8}$$

With this expression for the magnitude of d_3, and the fact that its angle relative to the z-axis is $\theta - \nu$, we can give $W(\theta)$ and $h(\theta)$ as follows.

$$W(\theta) = -[a - d_2 - d_3 \cos(\theta - \nu)] \tag{9}$$

$$h(\theta) = a \sin\theta - d_3 \sin(\theta - \nu).^{10} \tag{10}$$

In addition, it can be shown that the radius of curvature ρ of a section of wavefront is[11]

$$|\rho| = \frac{\left[1 + \left(\frac{dW}{dh}\right)^2\right]^{3/2}}{\frac{d^2W}{dh^2}}. \tag{11}$$

---

10. The minus sign on the right-hand side of Eq. (9) follows a convention set out by P. L. Marston, "Geometrical and catastrophe optics methods in scattering," *Physical Acoustics,* forthcoming.
11. See Marston, op. cit., Eq. (109).

Some application of the calculus chain rule leads to

$$|\rho| = \frac{[h_\theta^2 + W_\theta^2]^{3/2}}{W_{\theta\theta} h_\theta - W_\theta h_{\theta\theta}}, \qquad \textbf{(12)}$$

where $h_{\theta\theta}$ indicates the second total derivative of h with respect to θ.

For any given value of θ, the appropriate point on the caustic surface is located by proceeding in the direction of the ray a distance equal to the radius of curvature (Figure 16).

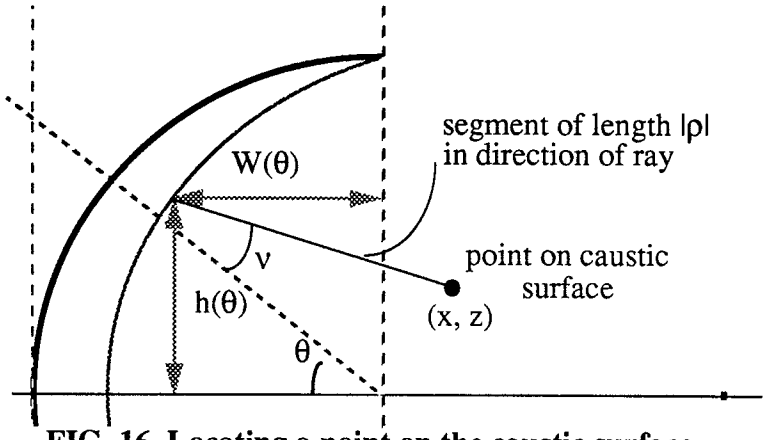

FIG. 16. Locating a point on the caustic surface

If that point is called (x, z), then

$$x = h(\theta) - |\rho| \sin(\theta - \nu) \qquad \textbf{(13)}$$

and

$$z = W(\theta) + |\rho| \cos(\theta - \nu)\,. \qquad \textbf{(14)}$$

If a large number of points on the wavefront, for values of θ such that $0 < |\theta| < \pi/2$, are examined in this way, then a picture of the caustic surface can be built up. Choosing more points yields finer detail, to whatever degree of detail is desired. The results of one such series of computations is shown in Figure 17. We summarize this section in Figure 18.

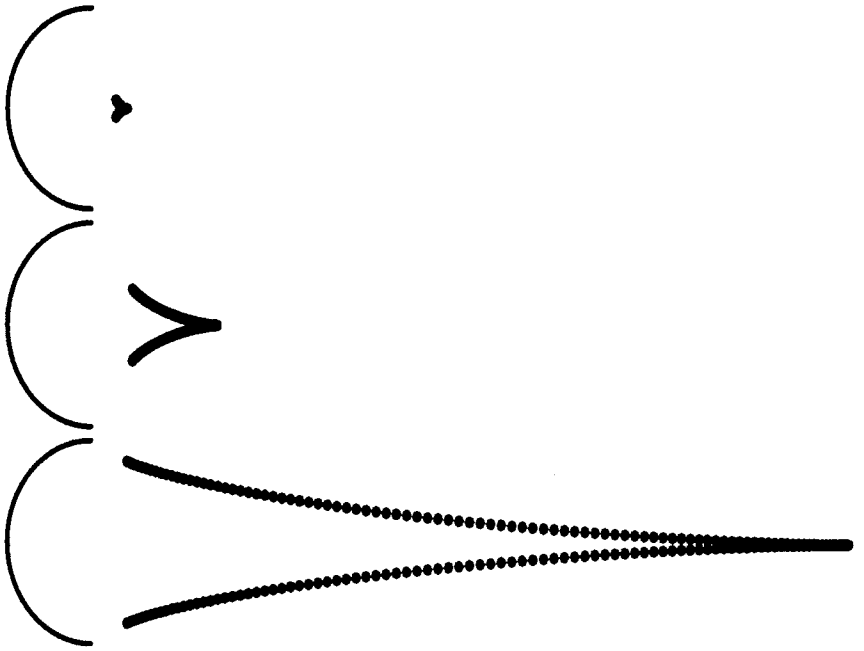

FIG. 17. Calculation[12] of the caustic curve for a hemispherical lens with increasing sound speed in the inner fluid and soundspeed ratios of 0.3, 0.6, and 0.9.

We have moved from Section I's more-or-less qualitative exposition of rays and caustics, to an elucidation of the notion of a wavefront. From there we moved to a quantitative treatment of the problem of describing the caustic surface in terms of the properties of the wavefront. We now move toward the full Kirchhoff calculations of the wavefield covering the skeleton whose location was just described.

12. See Appendix D for details of this calculation.

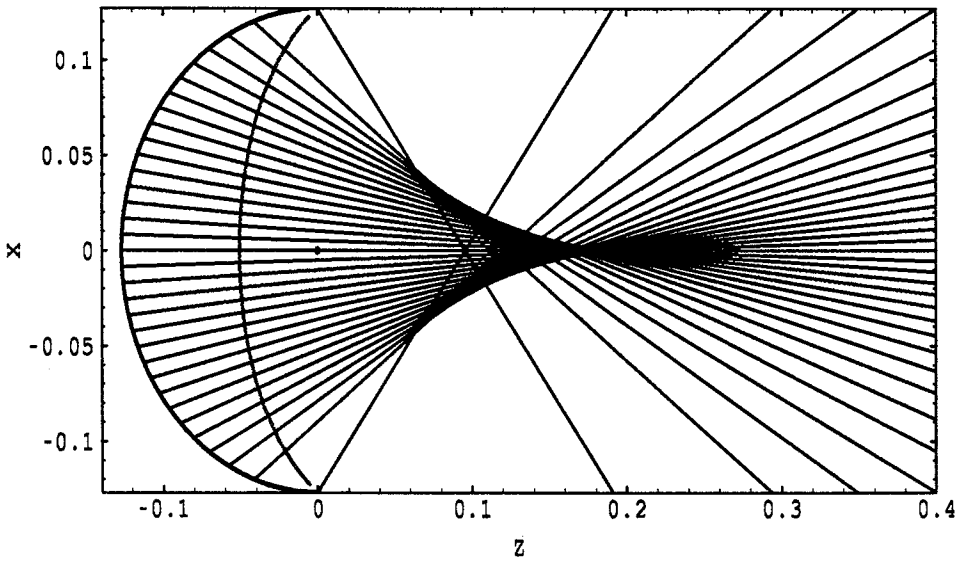

FIG. 18. Lens surface, wavefront, refracted rays, and caustic curve

B. Preliminaries to the Kirchhoff calculations

There are two sorts of preliminaries to deal with here: first, the nature of the Kirchhoff calculations, and then the initial conditions for the Kirchhoff calculations.

In the wave theory, propagation of sound through the acoustic lens cannot be treated just as a case of refraction at a spherical boundary between two different media. It becomes important that the lens has edges that can *diffract* the incident waves. In the language of geometrical acoustics, wavefronts that encounter the edge of the lens are not merely "clipped," but in addition the transmitted portions are "warped." Equivalently, the trajectories of rays passing near the lens's edge are "bent." This effect cannot be explained in terms of geometrical acoustics: it is not reflection or refraction. The interference of the so-called "boundary diffraction waves" with the unobstructed portion of the incident wave (the "geometrical wave") produces effects throughout the field of interest.[13] A method of obtaining the solution is embodied in the Kirchhoff integral theorem, with which we deal in Section III.C below. But first, the rudiments of Kirchhoff diffraction theory.

Consider each point on a wavefront as a source of secondary spherical wavelets, such that each spherical wavelet's amplitude is strongest in the wavefront's forward direction and zero in its

13. For a brief introduction to the idea of boundary diffraction waves, see E. Hecht and A. Zajac, *Optics* (Reading, Mass.: Addison-Wesley Publishing Co., 1974) pp. 392-393 and the references given there.

backwards direction, and such that the wavelets' phases have been shifted with respect to the wavefront's phase. Kirchhoff's diffraction theory holds that the propagation of the wavefront is the same as the propagation of the superposition of the wavelets. (This is the so-called Huygens-Fresnel principle: Kirchhoff's contribution was to put the insights of Huygens and Fresnel on a firmer mathematical and wave-theoretical footing.) Figure 19 shows a time-series of the so-called Huygens construction for the propagation of a wavefront, the earliest stage being shown at the top-left, the latest at the bottom-right.

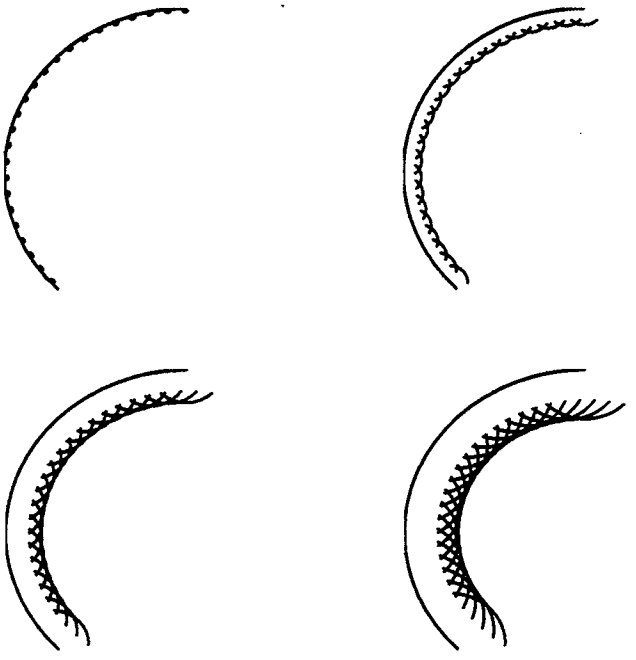

FIG. 19. Huygens construction for the propagation of a wavefront

If we let the number of wavelets go to infinity, adjust the phase, and weight the wavelets properly for direction (the so-called obliquity factor, which we owe to Fresnel) and amplitude, the resulting superposition approximates observed phenomena to considerable accuracy. The means for computing such a superposition of weighted wavelets is the Kirchhoff integral, which is known to be valid at a relatively large distance from a relatively large aperture.[14] The standard of largeness is a wavelength, as is typical in wave theory. For the centimeter-scale wavelengths treated in this report, the dimensions of the acoustic lens to be examined are large.

In making the Kirchhoff calculations for the acoustic lens, it turns out to be advantageous to choose as a set of initial conditions the pressures on the exit plane of the lens, P (s, z = 0). These conditions can be obtained by using ideas from geometrical acoustics in tandem with ideas from a richer wave theory of acoustics. Consider the following figure.

---

14. See, e.g., W. C. Elmore and M. A. Heald, *Physics of Waves* (New York: Dover Publications, Inc., 1969) pp. 326-340; J. W. Goodman, *Introduction to Fourier Optics* (San Francisco: McGraw-Hill Book Co., 1968) pp. 31-42; Ref. 7, pp. 215-217; references cited in those works.

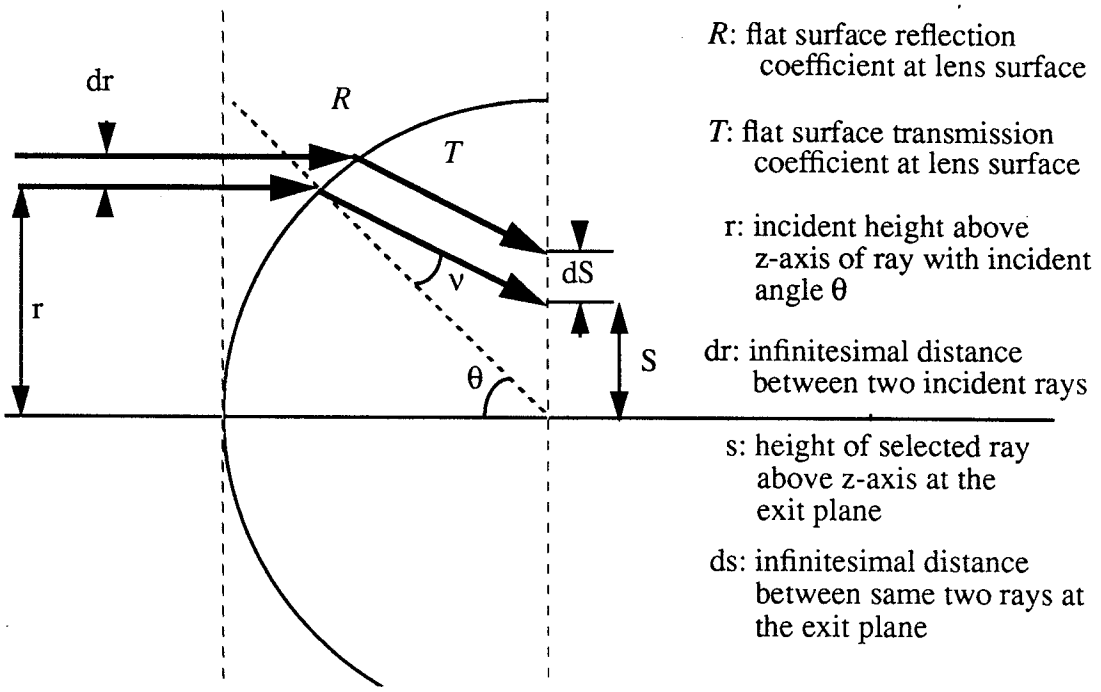

FIG. 20. Definitions used in deriving the array of pressures on the exit plane

The ratio *dr/ds* is an index of the extent to which pressure amplitudes at the entrance plane are "squeezed" by the lens on their passage to the exit plane. *T* is an index of the pressure amplitude transmitted across the lens surface, and not reflected. (We ignore any absorption in the system.) If the incident wave has unit amplitude, one can say that the section of the wave at *ds* has amplitude *T dr/ds*. Propagation through the lens affects the wave's phase: including a phase propagation contribution η, the delay of the ray compared to a ray incident at $r = 0$, gives

$$P(s,z=0) = T\left(\frac{dr}{ds}\right)^{1/2} e^{i\eta}. \qquad \textbf{(15)}$$

The first term in this expression for the pressures at the exit plane (*T*, the transmission coefficient) is derived by solving the wave equation for a flat surface using the boundary conditions represented by the lens. It is a product of wave theory. The second two are derived by geometrical arguments--essentially Snell's law, which gives us ν, and the shape of the lens. In the present effort, all are then expressed in terms of *s*, giving essentially

$$P(s,z=0) = T(s)\left(\frac{dr}{ds}(s)\right)^{1/2} e^{i\eta(s)}. \qquad \textbf{(16)}$$

More insight into the caustic and the limitations of the geometrical approach can be gotten by considering what happens to the geometrical acoustics pressures as they are propagated forward past the exit plane into the focusing region. An index of the behavior of these pressures is the behavior of the ratio *dr/ds*: as it increases, the pressures increase. And, if we were to move the exit plane in the positive z-direction, the ratio would change, because the denominator *ds* would grow smaller, approaching 0. Where it reaches 0—where two adjacent rays meet, as it were—the geo-

metrical acoustics pressure diverges to infinity. The locus of points where this happens is, again, the caustic surface.The compound figure below was obtained by plotting the variable term $1/ds$ in the caustic region. Notice that at some spatial points, the term $1/ds$ is triple-valued. This is a result of the fact that, at such points, three sets of rays arrive at each point, as shown in part b) of the figure. These results indicate that throughout this region interference and diffraction play an essential role in determining the pressure seen.

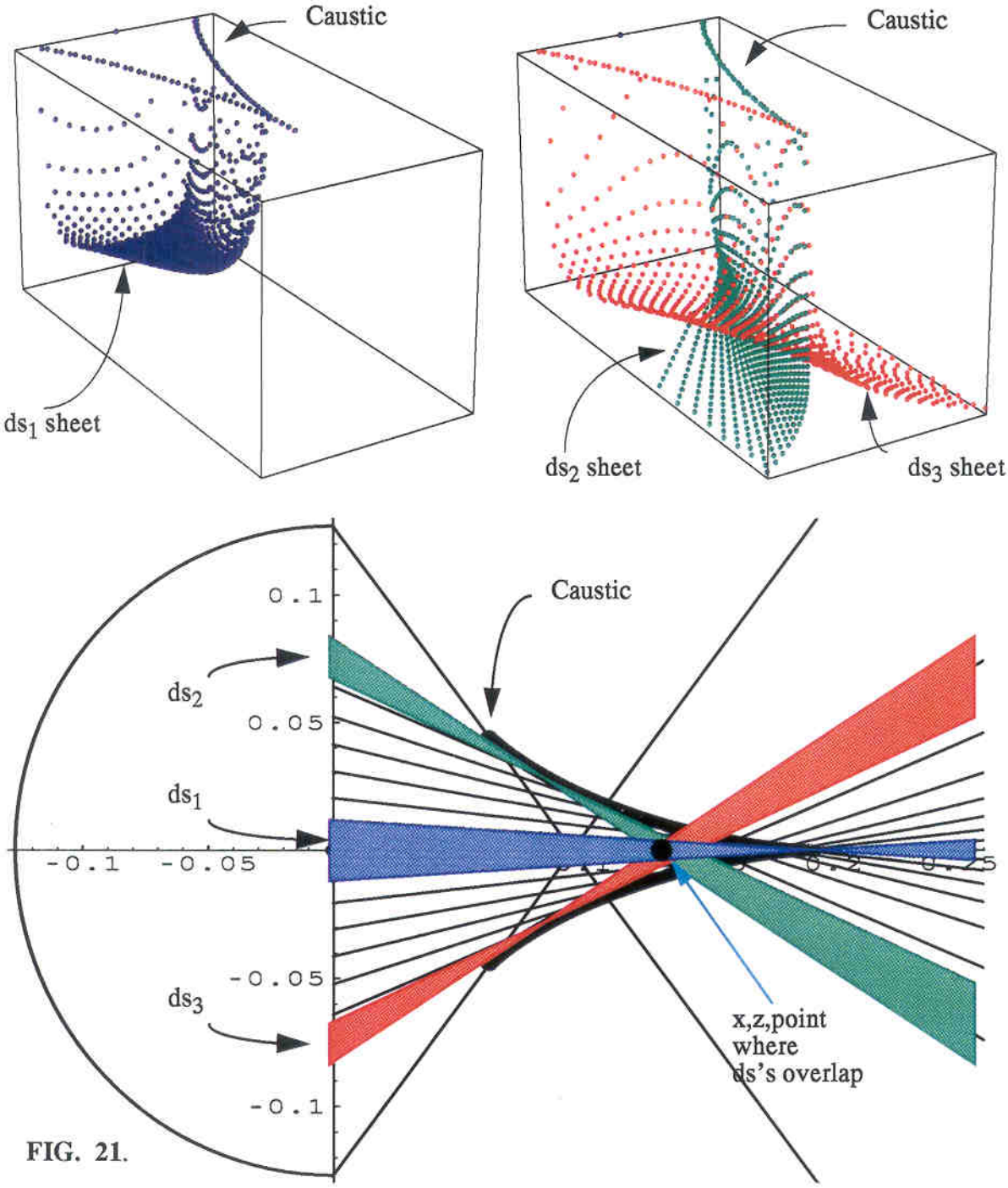

FIG. 21.

C. Calculation of the wavefield

A statement of Kirchhoff's integral theorem, in terms of the variables given in Figure 14 is the following: the pressure at any point (x, ψ, z) past the exit plane is

$$P(x, \psi, z) = -\frac{1}{2\pi}\iint P(s, z=0)\frac{\partial}{\partial z}\left(\frac{e^{ik_i R(s, \phi, z, \psi)}}{R(s, \phi, z, \psi)}\right) s\,ds\,d\phi \quad , \qquad \textbf{(17)}$$

where

$k_i = (2\pi f)/c_i$, with f the frequency of the sound being used (here, 100 kHz), and

e^{ikR}/R is the point-source Green's function—a way of describing the perturbation of the pressure field that generates the waves—with R the distance between a given point on the exit plane and the point of interest in the pressure field.

Assuming R is much larger than a wavelength (it is on the order of 10 centimeters), we can approximate the integral equation above as

$$P(x, \psi=0, z) \approx -\frac{ik_i z}{2\pi}\iint P(s, z=0)\frac{e^{ik_i R(s, \phi, x, z)}}{R^2(s, \phi, x, z)} s\,ds\,d\phi \quad . \qquad \textbf{(18)}$$

In Eq. (18) we have set $\psi = 0$ since symmetry implies that the pressure field will be the same in all ψ planes. A last bit of substitution yields the final form of the integral. Consider Figure 22.

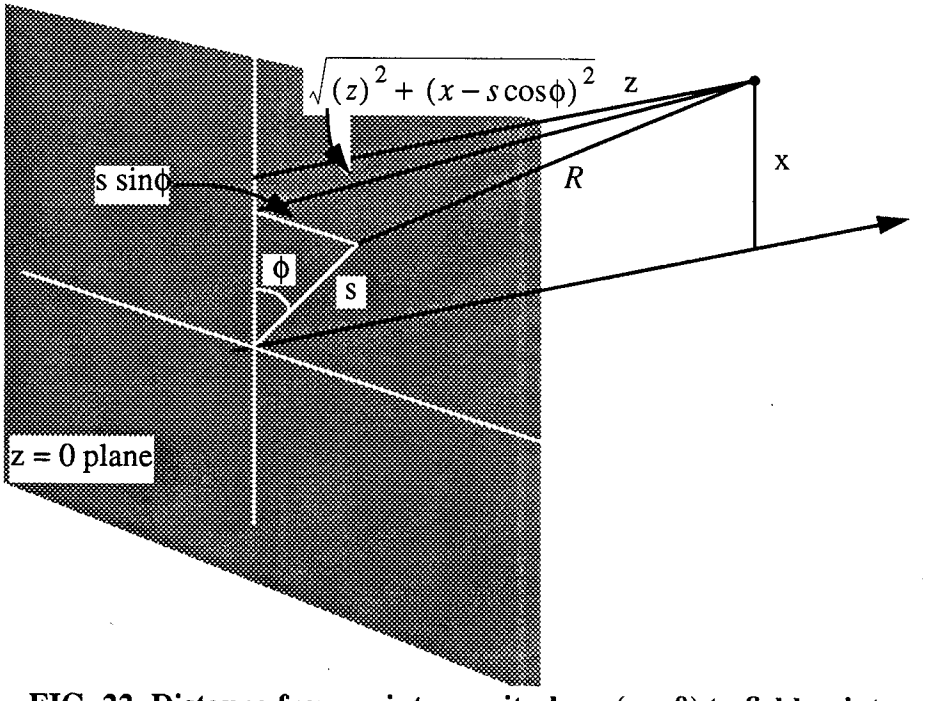

FIG. 22. Distance from point on exit plane (z = 0) to field point

From it we see that

$$R = \sqrt{z^2 + (x - s\cos\phi)^2 + (s\sin\phi)^2} \tag{19}$$

$$= \sqrt{z^2 + x^2 + s^2 - 2xs\cos\phi}\ . \tag{20}$$

Finally, with this and the expression for the pressure on the exit plane in Eq. (16), we have

$$P(x;\psi=0;z) \approx \frac{-ik_i z}{2\pi} \int_0^{2\pi} \int_0^a T(s) \left(\frac{dr}{ds}\right)^{1/2} e^{i\eta(s)} \frac{e^{ik_i\sqrt{z^2 + x^2 + s^2 - 2xs\cos\phi}}}{(z^2 + x^2 + s^2 - 2xs\cos\phi)} s\,ds\,d\phi. \tag{21}$$

This equation has been solved numerically for an array of positions (x, z) in the vicinity of the caustic in order to obtain a view of the wavefield of the lens. Appendix E gives details of the calculation of $T(s)$, $(dr)/(ds)$, and $e^{i\eta(s)}$. Typical results are shown in Figures 23 and 24.

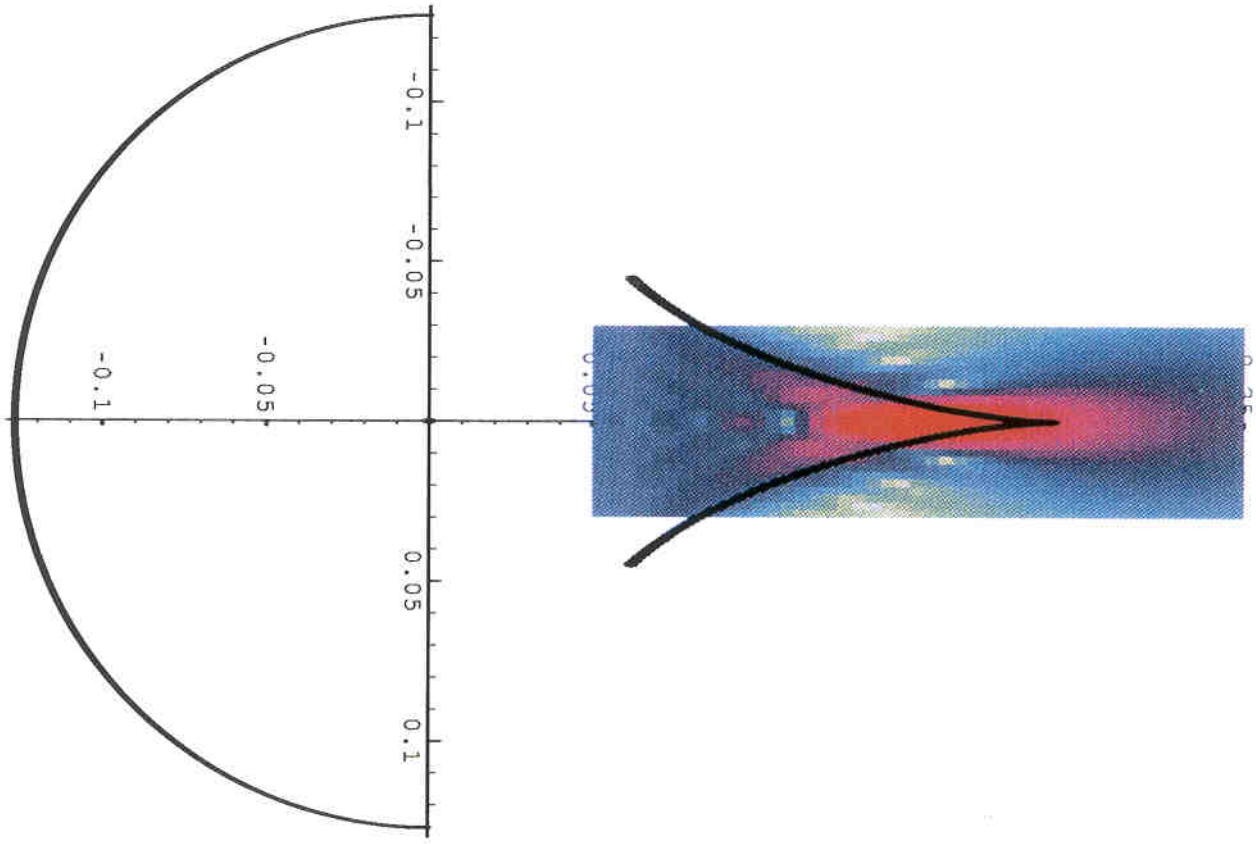

FIG. 23. Pressure field near the caustic

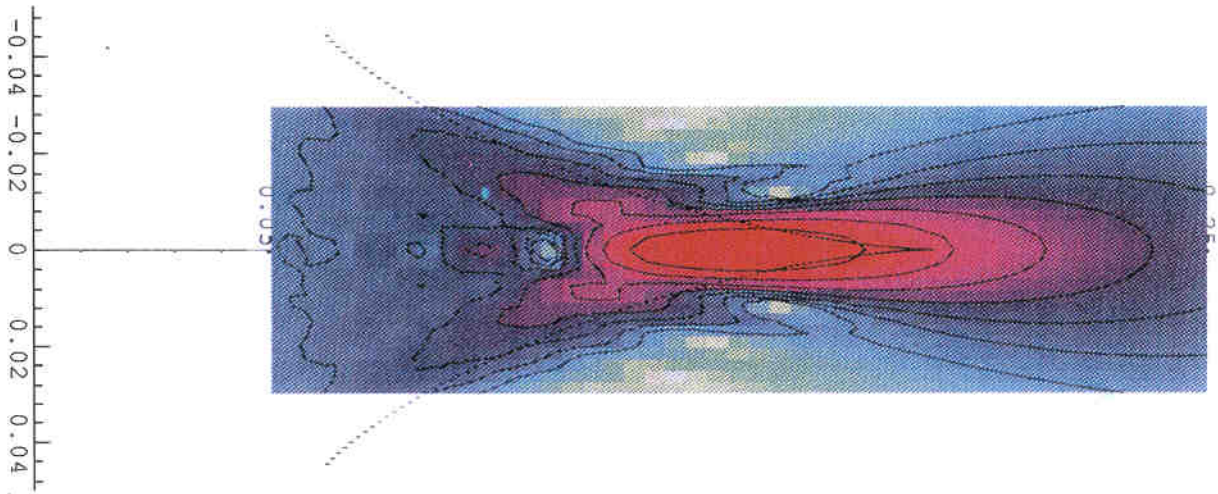

FIG. 24. Detail from Figure 21, with pressure contours added

Figures 23 and 24 show the pressure field for the region near the caustic, calculated for a lens whose sound-speed ratio c_i/c is about 0.6.[15] Red indicates high pressure levels, and light green low pressure levels. The contours added to Figure 24 are at 3 dB intervals. Notice that there are no pathological, infinite pressure values generated by the wave calculations. The central ellipse in Figure 24 indicates a maximum pressure region inside the caustic curve. There are sharply declining pressures to either side (in the plus and minus x-directions) and gently declining pressures in back and in front (in the plus and minus z-directions). But even though the geometrical-acoustics' caustic is softened by the wave covering, it is not eliminated. Knowing just the form of the lens's caustic, or the plot of $1/ds$, a person could easily infer much of the actual pressure field predicted by the wave theory and measured in fact.

IV. Summary

We began by introducing the idea of an acoustic lens, and by examining properties of focusing acoustical systems: mirrors and then lenses. The geometrical approach to acoustics was sketched, and some of its limitations discussed. The crucial notion of a system's caustic was explored. A hybrid geometrical acoustics/wave acoustics approach to the problem was described and used. Equation (21) is the final result of this approach, giving the Kirchhoff wave integral approximation for the pressure past the exit plane of the lens. With it, the divergences inherent in the geo-

15. The parameters used are those for APL's acoustic lens: c_i/c =0.6012, a=0.127 m. The sound frequency is 100 kHz. See Figure 9 for a plot of refracted rays in such a lens.

metrical acoustics approach have been eliminated. However, the pressure at the exit plane was determined by using the geometrical acoustics approach, considerably simplifying the wave theory calculations and allowing a good and valid physical picture of the wave propagation into the region of interest.

It is important to note that, up to this point, the effect of the lens shell and the beam pattern of the retinal elements have not been taken into account. Inclusion of these effects are straightforward in principle.

Appendix A: Generating Figures 3 Through 8

These figures were generated using two variations of a program written in Mathematica. The program had three components: define the reflector's surface; for given points of incidence upon the reflector's surface, compute the slope and remote endpoint of the reflected ray; and, using the information computed, draw the graphics.

The program varied only in the definitions of the reflectors' surfaces: Diagrams 2 through 6 used a parametric version of $z = Ax^2 + Bx^4$; Figure 8 used a parametric version of $\pm z = \sqrt{r^2 - x^2}$. A, B, and r were variable parameters, as was the range of x.

The second component of the program had a loop structure. Each iteration of the loop did the following:

1. picked a point of incidence—chosen to be evenly spaced in the z-dimension
2. calculated the slope of the reflector at that point—using the derivative of the defining equation of the reflector
3. calculated the angle between the incident ray and the reflector at that point:
   a) for this program, all incident rays were parallel to the principal (i.e., the x-) axis and thus had slope 0—it is considerably messier to allow variation in the slope of the incident rays, but luckily it is unnecessary here
   b) the angle was calculated using a result from analytic geometry; the angle θ_{12} between lines l_1 and l_2 having slopes m_1 and m_2, respectively, is

$$\theta_{12} = \tan^{-1}\left(\frac{m_2 - m_1}{1 + m_2 m_1}\right) \qquad \textbf{(22)}$$

4. calculated the slope of the reflected ray at that point, m_3, using another form of the result above:
   a) call the angle between the reflector and the reflected ray θ_{23}; we know $\theta_{23} = \theta_{12}$
   b) it follows that

$$m_3 = \frac{m_2 + \tan\theta_{12}}{1 - m_2 \tan\theta_{12}} \qquad \textbf{(23)}$$

5. found the coordinates of the point to be used as the endpoint of the segment of the reflected ray:
   a) we know the endpoint of the reflected ray—the point of incidence on the reflector
   b) choose the z-coordinate of the endpoint of the segment of the reflected ray that will be drawn—its magnitude is a matter of aesthetics, but its sign will be *opposite* to the z-coordinate of the point of incidence for the reflections of interest to us: that is, we are interested only in rays that reflect across the principal axis
   c) using the point-slope form of the equation of a line, choose the associated x-coordinate
6. used the two endpoints now known to describe a line segment graphics primitive
7. appended the result to a table of such primitives
8. returned.

The output component of the program combined a plot of the reflector's surface with a plot of

the table of descriptions of reflected rays stored by the loop. Anomalous reflected rays are possible with the routine described above, i.e., marginal rays which would in fact have reflected multiply. But by constraining the range of incident points closer to the x-axis, these rays can be eliminated. They are not necessary for present purposes.

Appendix B: Generating Figures 10 and 11

These figures were again generated by a program written in Mathematica. As this program was a specialized version of a program used later in the wave calculations, its logic was rather different from the program described in Appendix A. However this program, too, had three components: define the lens; for given angles of refraction, compute the point of incidence and a remote point on the refracted ray; and, using the information computed, draw the graphics.

We limited ourselves to considering hemispherical acoustic lenses—i.e., ones with sections in the x-z plane that were semicircles.[16] Here, the variable parameters for the lens were the radius of the semicircle and the index of acoustic refraction.

Again, the second component of the program was a loop. Exploiting the fact that there is a degree of circular symmetry to the problem, computations tended to be trigonometric. For given numbers of values of the angle of incidence, ν, between positive and negative $\pi/2$, the loop

1. computed the value of the angle of incidence, θ, using Snell's law
2. computed the refracted ray's intersection with the x-axis, S, in terms of the angle $(\theta - \nu)$
3. found the coordinates of the point of incidence on the semicircle
   a) the x-coordinate = $\pm\,(radius)\ (\sin\theta)$
   b) the z-coordinate = $(radius)\ (\cos\theta)$
4. found the coordinates of a remote point on the refracted ray
   a) the x-coordinate is some constant, C, chosen to make a pleasing display
   b) the z-coordinate = $C\tan(\theta - \nu) - S$
5. created a line graphics primitive between the two points chosen
6. appended the graphics primitive to a table of such graphics primitives
7. returned.

The output was produced as described in Appendix A.

16. Geometrical acoustic theory suggests that incident rays parallel to the principal axis can be focused without primary aberration by a lens whose shape is ellipsoidal or hyperboloidal, depending upon the index of acoustic refraction. The drawback of such a lens is that this is true only for paraxial rays: i.e., such a lens has a very narrow field of view. The reader might find it amusing to write a program to domesticate this claim.

Appendix C: Creating Figure 12

The point here is to locate the caustic produced by a reflecting surface, as opposed to that produced by the lens (Figure C.1).

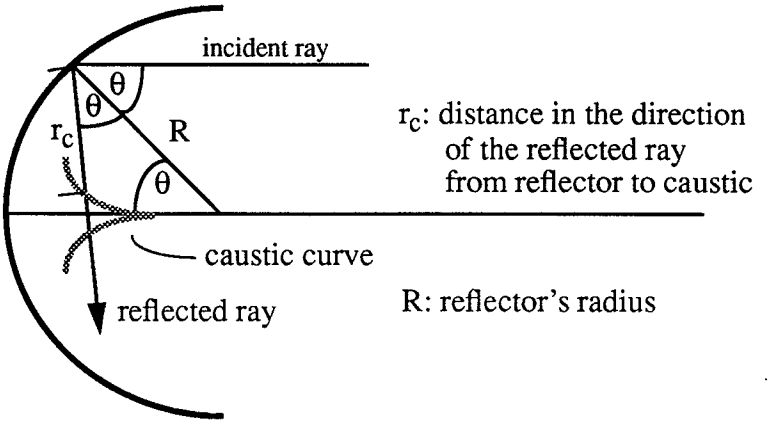

FIG. C.1. Terms for Appendix C

The equation for locating the tangential caustic is derived by[17]:

$$\frac{1}{r_c} = -\frac{2}{R\cos\theta}. \qquad (24)$$

(The equation has been specialized to the case of an object at infinity.) Given expressions for points on the reflector's surface and for the x- and z-components of r_c—i.e., ($r_c \cos(\pi/2 - 2\theta)$, $r_c \sin(\pi/2 - 2\theta)$) for $\theta < \pi/4$—the caustic curve is easily computed. Note that the authors' expressions--not the specialized versions given above—can serve for noninfinite object distances and for refracting surfaces. Figure 12 was generated by a short program written in Mathematica.

17. D. G. Burkhard and D. L. Shealy, Applied Optics 21, 3299 (1982) and the references cited therein

Appendix D: Locating the Caustic Surface for the Acoustic Lens

This was a two-step process: first, locate the wavefront; then, from the curvature of the wavefront, locate the caustic. While it is intuitively appealing to describe the wavefront in terms of the parameter θ, the angle of incidence, it turns out to be computationally advantageous to describe the wavefront in terms of ν, the angle of refraction. The change of parameters is accomplished using Snell's law.

$$\sin\nu = \frac{c_i}{c}\sin\theta \tag{25}$$

$$\theta = \sin^{-1}\left(\frac{c}{c_i}\sin\nu\right). \tag{26}$$

We can obtain all our results in terms of ν using the above expression for θ. Thus

$$h(\nu) = \operatorname{asin}\left[\sin^{-1}\left(\frac{c}{c_i}\sin\nu\right)\right] - \tag{27}$$

$$\frac{c_i}{c}\operatorname{acos}\left[\sin^{-1}\left(\frac{c}{c_i}\sin\nu\right)\right]\sin\left[\sin^{-1}\left(\left(\frac{c}{c_i}\sin\nu\right)-\nu\right)\right]$$

$$W(\nu) = -\left(\operatorname{acos}\left[\sin^{-1}\left(\frac{c}{c_i}\sin\nu\right)\right] - \right. \tag{28}$$

$$\left.\frac{c_i}{c}\operatorname{acos}\left[\sin^{-1}\left(\frac{c}{c_i}\sin\nu\right)\right]\cos\left[\sin^{-1}\left(\frac{c}{c_i}\sin\nu\right)-\nu\right]\right)$$

The change of variables and the calculus involved in obtaining the expressions for $|\rho|$ are as follows.

$$|\rho| = \frac{\left[1+\left(\frac{dW}{dh}\right)^2\right]^{3/2}}{\frac{d^2W}{dh^2}} \tag{29}$$

$$= \frac{\left[1 + \left(\frac{dW}{d\nu}\frac{d\nu}{dh}\right)^2\right]^{3/2}}{\frac{d}{d\nu}\left(\frac{dW}{d\nu}\frac{d\nu}{dh}\right)\frac{d\nu}{dh}}$$

$$= \frac{\left(\frac{d\nu}{dh}\right)^3\left[\left(\frac{dh}{d\nu}\right)^2 + \left(\frac{dW}{d\nu}\right)^2\right]^{3/2}}{\frac{d^2W}{d\nu^2}\left(\frac{d\nu}{dh}\right)^2 + \frac{dW}{d\nu}\left[\frac{d}{d\nu}\left(\frac{dh}{d\nu}\right)^{-1}\right]\frac{d\nu}{dh}}$$

$$= \frac{\left[\left(\frac{dh}{d\nu}\right)^2 + \left(\frac{dW}{d\nu}\right)^2\right]^{3/2}}{\frac{d^2W}{d\nu^2}\frac{dh}{d\nu} - \left(\frac{dW}{d\nu}\right)\left(\frac{dh}{d\nu}\right)^3\left(\frac{d\nu}{dh}\right)\left[\left(\frac{d\nu}{dh}\right)^2\frac{d^2h}{d\nu^2}\right]} \qquad \textbf{(30)}$$

$$|\rho| = \frac{[h_\nu^2 + W_\nu^2]^{3/2}}{W_{\nu\nu}h_\nu - W_\nu h_{\nu\nu}} \qquad \textbf{(31)}$$

The plotting was, again, accomplished by a program written in Mathematica. Each of the terms on the right-hand side of the expression given immediately above for $|\rho|$ was derived and translated into computer code. Then, for a variety of values of ν—corresponding, of course, to a range of angles of incidence—the distance $|\rho|$ was computed and added to the point (h, W) along the ray direction. This located the point (x, z) mentioned in the text.

Appendix E: The Pressures at the Exit Plane

The expression given in the main body of the text for the pressures at the exit plane was $P(s,z=0) = T(dr/ds)\,e^{i\eta}$. In order to compute P, each of the factors in the right-hand side of the equation was first expressed in terms of ν, then numerically re-expressed in terms of s-dependence.

1. Transformations into terms of ν

Solving the wave equation for the boundary between the two media, with the approximation that the boundary can be treated as flat, which is reasonable on the scale of the wavelengths used here, gives

$$T = \frac{2\rho_i c_i \cos\theta}{\rho c \cos\nu + \rho_i c_i \cos\theta}, \tag{32}$$

where ρ is the density of the fluid outside the lens, and ρ_i is the density inside. In terms of ν this is

$$T(\nu) = \frac{2\rho_i c_i \cos\left[\sin^{-1}\left(\frac{c}{c_i}\sin\nu\right)\right]}{\rho c \cos\nu + \rho_i c_i \cos\left[\sin^{-1}\left(\frac{c}{c_i}\sin\nu\right)\right]}. \tag{33}$$

For the ratio of entrance-plane/exit-plane dimensions dr/ds, elementary calculus allows us to write

$$\frac{dr}{ds} = \frac{dr}{d\nu} \Big/ \frac{ds}{d\nu}. \tag{34}$$

The propagation phase delay η can be found as follows. Please refer to Figure 20 and to Figure E.1.

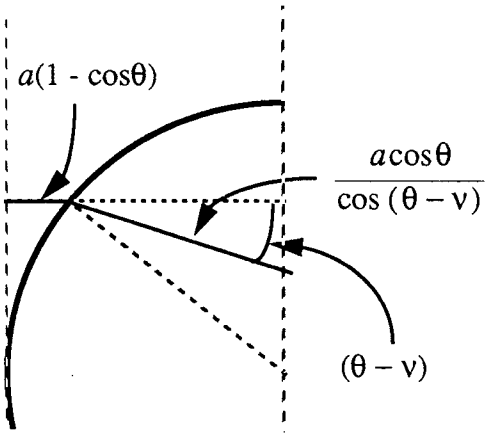

FIG. E.1. Terms for finding propagation phase delay η

Propagation phase delay is just the phase shift, relative to some standard, a wave undergoes as it travels between two points--how much older the wave gets, as it were

$$\textit{phase delay} = (2\,\pi\,\textit{distance}) \,/\, \textit{wavelength}. \tag{35}$$

For a ray with $r = 0$ (i.e., $\theta = 0$) going from the entrance plane to the exit plane, the phase delay is $k_i a$, where k_i is the wave number inside the lens, $2\pi/\lambda_i$, and a is the lens's radius. The propagation phase delay for rays incident at $r \neq 0$ consists of two parts: the phase delay outside the lens and the phase delay inside the lens. For the former we have $ka(1 - \cos\theta)$; for the latter, $k_i \left(\frac{a\cos\theta}{\cos(\theta - \nu)}\right)$.

We choose as our standard the time delay for a ray at $r = 0$. Thus

η = *(delay of* $r \neq 0$ *ray) - (delay of* $r = 0$ *ray)*

$$= k_i \left(\frac{k}{k_i}\right) a(1 - \cos\theta) + k_i \frac{a\cos\theta}{\cos(\theta - \nu)} - k_i a$$

$$= k_i\, a\left[\frac{c_i}{c}(1 - \cos\theta) + \frac{\cos\theta}{\cos(\theta - \nu)} - 1\right]. \tag{36}$$

Or, rewriting in terms of ν,

$$\eta(\nu) = k_i a\left[\frac{c_i}{c}\left(1 - \cos\left[\sin^{-1}\left(\frac{c}{c_i}\sin\nu\right)\right]\right)\right] + \frac{\cos\left[\sin^{-1}\left(\frac{c}{c_i}\sin\nu\right)\right]}{\cos\left[\sin^{-1}\left(\frac{c}{c_i}\sin\nu\right) - \nu\right]} - 1. \tag{37}$$

We can give the distances r and s above the z-axis at the entrance and exit planes, respectively, as

$$r = a\sin\theta$$

$$= a\sin\left[\sin^{-1}\left(\frac{c}{c_i}\sin\nu\right)\right] \tag{38}$$

$$s = a\,[\sin\theta - \cos\theta \tan(\theta - \nu)]$$

$$= a\left(\sin\left[\sin^{-1}\left(\frac{c}{c_i}\sin\nu\right)\right] - \cos\left[\sin^{-1}\left(\frac{c}{c_i}\sin\nu\right)\right]\tan\left[\sin^{-1}\left(\left(\frac{c}{c_i}\sin\nu\right) - \nu\right)\right]\right). \tag{39}$$

We can now write

$$P(\nu, z=0) = T(\nu)\left(\frac{dr}{d\nu} \Big/ \frac{ds}{d\nu}\right)^{1/2} e^{i\eta(\nu)}. \tag{40}$$

2. Numerical fitting of expressions in terms of ν to terms of s

In order to translate Eq. (40) into terms of s, data tables of the form

$$\{s(\nu), \eta(\nu)\},\ \{s(\nu), \left(\frac{dr}{d\nu} \Big/ \frac{ds}{d\nu}\right)^{1/2}\},\ \{s(\nu), T(\nu)\} \tag{41}$$

were prepared. They were used to determine mean-square fits to the following:

$$\eta(s) = A_1 + B_1 s + C_1 s^2 + D_1 s^3 + E_1 s^4 \tag{42}$$

$$T(s) = A_2 + B_2 s + C_2 s^2 + D_2 s^3 + E_2 s^4 + F_2 s^5 + G_2 s^6 \tag{43}$$

$$\frac{dr/d\nu}{dr/d\nu}(s) = A_3 + B_3 s + C_3 s^2 + D_3 s^3 + E_3 s^4 + F_3 s^5 + G_3 s^6 + H_3 s^7 + I_3 s^8 \tag{44}$$

Parametric plots of the data tables plotted against the mean-square fits confirm the fitting procedure.

The functions $\eta(s), T(s)$, and $\frac{dr/d\nu}{ds/d\nu}(s)$ can be put into Eq. (40), and then (40) substituted into Eq. (18), to obtain our final expression

$$P(x;\psi=0;z) \approx \frac{-ik_i z}{2\pi}\int_0^{2\pi}\int_0^{a} T(s)\left(\frac{dr}{ds}(s)\right)^{1/2} e^{i\eta(s)} \frac{e^{ik_i\sqrt{z^2+x^2+s^2-2xs\cos\phi}}}{(z^2+x^2+s^2-2xs\cos\phi)} s\,ds\,d\phi. \tag{45}$$

Equation (45) is solved numerically for an array of positions (x, z) in the vicinity of the caustic to obtain a view of the diffraction field of the acoustic lens, for specified values of

sound speeds: c, c_i

lens radius: a

frequency of sound waves: f.

It was necessary to write a FORTRAN program to execute the solution: Mathematica proved to be

very slow in executing the algorithms chosen. A copy of the FORTRAN program for the parameters used in generating Figure 24 is given in Appendix F.

Appendix F: FORTRAN CODE

```
c       this program calculates the following integral
c
c                  b    d
c                  |    |
c                  |    |
c                  |    | f(x,y) dxdy
c                  |    |
c                  |    |
c              y=a  x=c
c

c       and a composite Simpson's rule of order nbase
c       for the both integrals
c       (subroutine simsim)

c       NOTE: 'function fsimp(x,y)' contains the integrand.
c       it is actually accessed in subroutine sim
c
c.....................................................
        real*8 a,b,c,d,rho,z
        complex*16 soln
        integer nbase1,nbase2
        common rho,z



        a=0.0
        c=0.0
        b=6.28318
        d=.127
        nbase1=50
        nbase2=50

        do 1 i=1,25

         rho=-0.03+(i-1)*0.06/24.0

         do 2 j=1,45

          z=.05+(j-1)*0.20/44.0
          call simsim(a,b,c,d,nbase1,nbase2,soln)
          write(20,*) ABS(soln)


 2        continue

 1       continue

        end



c@@@@@@@@@@@@@@@@@@@@@@@@@@@@@@@@@@@@@@@@@@@@@@@@@@@@@@@@@@@@@@@@@@@
        function fsimp(x,y)
        real*8 x,y,pi,seta,sTcoeff,sarearatio,freq,
     &         rho,z,lensspeed
        complex*16 fsimp,qi
        common rho,z
```

```
      pi = 3.141592654
      qi = CMPLX(0.d0,1.d0)

      freq=100000.0

       lensspeed=890.37


       sTcoeff=0.74968 - 1.23551e-12*x -
     &           21.2564*x**2 - 1.91763e-10*x**3
     &           - 4382.73*x**4 + 9.38765e-9*x**5
     &           + 174919.*x**6

       seta=0.0886702 - 1.24116e-12*x - 1964.59*x**2
     &        + 8.38885e-13*x**3 - 18100.6*x**4

       sarearatio=1.28591 + 2.01206e-11*x - 12.1853*x**2
     &              - 9.98851e-10*x**3 - 11323.9*x**4 +
     &              1.43113e-8*x**5 + 577842.*x**6 +
     &              9.47178e-8*x**7 - 7.97507e6*x**8


      R=SQRT(rho**2 + x**2 + z**2 - 2.*rho*x*Cos(y))

      fsimp =-qi*EXP(qi*2*pi*freq*R/lensspeed
     &         +qi*seta)*freq*x*z*sarearatio*sTcoeff/
     &           (lensspeed*R**2)


      return
      end


c@@@@@@@@@@@@@@@@@@@@@@@@@@@@@@@@@@@@@@@@@@@@@@@@@@@@@
      subroutine simsim(a,b,c,d,nbase1,nbase2,soln)

c     This program computes the following integral
c
c       y=b x=d
c        |   |
c       |   |
c       |   | f(x,y) dxdy
c       |   |
c      |   |
c    y=a x=c
c
c     via the Simpson composite integration formulas
c     for both integrals:
c                                          n-1
c     (b-a)/6n { f(a) + f(b) + 2 sum  f(a + 2s*(b-a)/2n )
c                                   s=1
c                               n-1
c                        + 4 sum  f(a + (2s+1)*(b-a)/2n )   }
c                              s=0
c
c     for 2n+1 basepoints from y0=a, y1, ..., y2n=b
c     and h=(b-a)/2n, where h is the resolution of the
```

```
c       integration formula.
c
c       (Carnahan, Luther and Wilkes, 1969, p79)*
c
c       function f(x,y) is in subroutine simp
c.....................................................................
        real*8 y1,y2,a,b,c,d,h
        complex*16 soln,f1,f2,fa,fb


        h = (b-a)/(2.*float(nbase1))


        y2 = a+h
        call simp(c,d,nbase2,y2,soln)
        soln = 4.d0*soln

        do 4 i=1,nbase1-1

        y1 = a + h*float(2*i)
        y2 = a + h*float(2*i+1)

        call simp(c,d,nbase2,y1,f1)
        call simp(c,d,nbase2,y2,f2)

        soln = soln + 2.d0*f1 + 4.d0*f2

 4      continue

        call simp(c,d,nbase2,a,fa)
        call simp(c,d,nbase2,b,fb)

        soln = (1.d0/3.d0)*h*( soln + fa + fb )

        return
        end



c@@@@@@@@@@@@@@@@@@@@@@@@@@@@@@@@@@@@@@@@@@@@@@@@@@@@@@@@@@@@@@@@@@@
        subroutine simp(c,d,nbase2,y,soln)

c       This program computes the following integral
c
c          d
c         |
c        |
c        | f(x,y) dx
c        |
c       |
c      c
c
c       via the Simpson composite integration formula:
c                                        n-1
c       (d-c)/6n { f(c) + f(d) + 2 sum   f(c + 2s*(d-c)/2n )
c                                       s=1
c                                  n-1
c                          + 4 sum  f(c + (2s+1)*(d-c)/2n )  }
```

*B. Carnahan, H.A. Luther, and J.O. Wilkes, Applied Numerical Methods, Wiley, New York, 1969

```
c                                   s=0
c       for 2n+1 basepoints from x0=c, x1, ..., x2n=d
c       and h=(d-c)/2n, where h is the resolution of the
c       integration formula.
c
c       (Carnahan, Luther and Wilkes, 1969, p79)
c.....................................................
        real*8 x1,x2,c,d,h,y
        complex*16 fsimp,soln

        h = (d-c)/(2.d0*float(nbase2))


        x2 = c + h
        soln = 4.d0*fsimp(x2,y)

        do 4 i=1,nbase2-1

        x1 = c + h*float(2*i)
        x2 = c + h*float(2*i+1)
        soln = soln + 2.d0*fsimp(x1,y) + 4.d0*fsimp(x2,y)

 4      continue

        soln = (1.d0/3.d0)*h*( soln + fsimp(c,y) + fsimp(d,y) )


        return
        end
```